High-Resolution ESR Imaging of $N@C_{60}$ Radicals on a Surface

EKATERINA SUHOVOY AND AHARON BLANK*
Schulich Faculty of Chemistry, Technion—Israel Institute of Technology, Haifa 32000, Israel

(Received 3 February 2008 and in revised form 16 March 2008)

Abstract. Electron Spin Resonance Microcopy (ESRM) is an imaging method capable of observing stable free radicals in small samples with a spatial resolution of ~1 micron. Currently this technique is pursued mainly for biological applications at room temperature and at relatively low static magnetic fields. Future progress, which involves the use of higher magnetic fields at cryogenic temperatures, could significantly improve sensitivity and resolution and thus make this method attractive to many solid-state and physical science applications. Here we consider a possible application of ESRM to the field of quantum computing employing Endohedral Nitrogen fullerene ($N@C_{60}$) molecules. In order to fully address the challenges of quantum computing, the resolution should be significantly improved to ~10 nm and the sensitivity should approach the single spin level. In the present work we show some preliminary results conducted with diluted $N@C_{60}$ samples. A 2D image of $N@C_{60}$ dispersed on a surface was obtained at a field of ~0.6 T and at room temperature. Under these conditions the current sensitivity of the ESRM system is around 10^7–10^8 spins, and due to the low enrichment factor of the $N@C_{60}$ sample (~10^{-6}), we were able to reach image resolution of only ~50 μm. Future steps that are taken in order to significantly improve resolution and sensitivity of the system are discussed. These include the use of highly concentrated samples to be measured at ~4 K and at a field of more than 1 T, which would lead to a resolution of ~100 nm and a sensitivity of ~100 spins.

INTRODUCTION

Endohedral Nitrogen fullerene ($N@C_{60}$) is a molecule containing a trapped nitrogen atom inside a fullerene C_{60} cage. This unique species has been studied extensively in recent years in aspects related to its physical, chemical, and magnetic properties.[1,2] $N@C_{60}$ was found to be very stable up to 260 ºC and can survive exohedral chemical addition reactions. Furthermore, as a consequence of its unique molecular structure, $N@C_{60}$ exhibits some special paramagnetic properties. The unpaired electron spins of this system have extremely long relaxation times with spin–spin relaxation time (T_2) measured to be ~20 μs, and the spin–lattice relaxation time (T_1) found to be ~0.1–1000 ms (depending on temperature).[3] Recently it was suggested that these paramagnetic properties can be very useful in the construction of a quantum computer based on $N@C_{60}$ qubits.[3–5]

Quantum computation (QC) is a relatively new field of science that aims at using the quantum properties of systems such as molecules, electrons, and photons to solve complex calculations. Problems such as factorization of large numbers or an item search in a large database can be solved much more efficiently by quantum computers than with classical computing devices. Furthermore, quantum computers could be used to simulate

*Author to whom correspondence should be addressed.
E-mail: ab359@tx.technion.ac.il

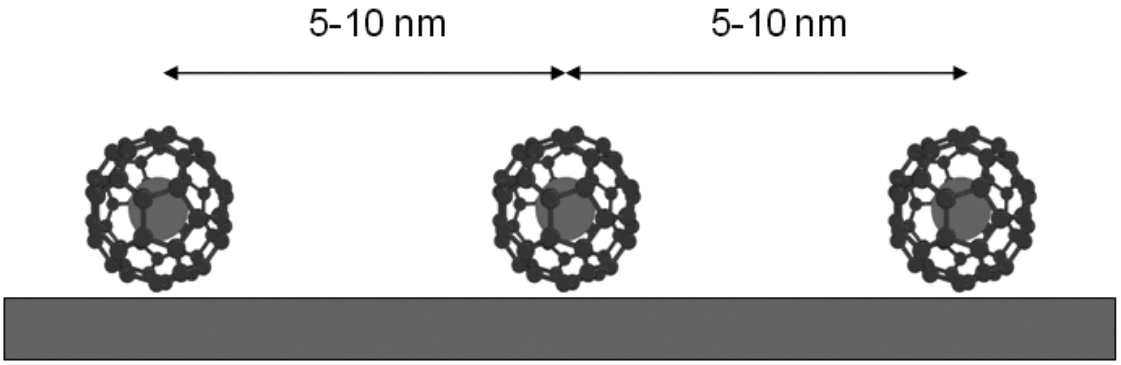

Fig. 1. An outline for a quantum computer based on the electron spins of $N@C_{60}$ as qubits.[3]

quantum experimental systems much better than any classical computer and also can be of significant importance in the field of cryptography.[6,7] In order to realize a working and useful quantum computing system, some basic requirements should be fulfilled.[8] The system must be comprised of several hundred quantum bits (qubit—analogous to the classical computer bit) coupled with each other and having long coherence (relaxation) time. There should be a mechanism for qubit initialization and quantum error correction, logic gates that perform calculations with the qubits, and an ability to read out the qubits values. Quantum computers with a small number of qubits, based on liquid NMR,[9] ion traps,[10] and silicon NMR,[11] were demonstrated. Nevertheless, these methods could be sufficient for the construction of a useful quantum computer, provided that the problem of scalability (i.e., going from few to many qubits) is solved.

Recently Harneit and coworkers presented a new approach for QC based on the use of $N@C_{60}$ arrays arranged on a surface (Fig. 1).[3] The long coherence time of this system makes it very attractive, and the physical arrangement of the spins presents a practical solution for the scalability problem that has risen in previous approaches. Furthermore, the environmental sheltering that the fullerene cage provides to the spin system inside it results in an excellent chemical and electrical isolation and it serves as an efficient mean for placing and arranging such large numbers of spins. The spins in the array are coupled to each other by means of the magnetic dipole interaction. Pulsed Electron Spin Resonance (ESR) can be employed for initializing the nitrogen spins (the qubits), performing logical quantum operations, performing error corrections, and, finally, reading out the state of the spins (the results of the calculation). This is a promising method, but there are some basic problems that should be solved before it can be realized in practice. So far, there has been no demonstration of any workable method for selecting and placing individual $N@C_{60}$ molecules in an ordered manner on the surface. Additionally, the current production efficiency of $N@C_{60}$ is quite low (under 10^{-5}) and requires many cycles of product purifications to reach satisfactory enrichment level.[12] Finally, the sensitivity and resolution of the spin detection and imaging capability need to be greatly improved from the current state-of-the-art, so that the signal of a specific single spin can be detected with a sufficient resolution of ~5–10 nm (see Fig. 1).

Our long-term work focuses on possible solutions to the last challenge through the development of high-sensitivity and high-resolution electron spin resonance detection and imaging techniques. Currently we have achieved micron-scale resolution at room temperature.[13] In the near future we aim at improving the detection sensitivity to the level of ~100 spins and the 2D spatial resolution to ~100 nm. To realize these goals we have developed ultrasensitive ESR resonators and imaging probes,[14] and plan to increase the static magnetic field to ~2 T and to reduce the temperature of measurement to ~4 K. Furthermore, fast pulse current drivers and optimized miniature gradient coils are being developed to facilitate the improvements in the spatial resolution to the nm scale.

In this paper, we shall present preliminary results of our ESR imaging work at room temperature and field of 0.6 T with solid $N@C_{60}$ molecules dispersed on the surface. First, continuous wave (CW) and pulsed ESR measurements of the $N@C_{60}$ spectrum and its measured T_1 and T_2 values are presented. Following that, the results of the 2D ESR micro-imaging of the $N@C_{60}$ sample are shown. At present, due to the low enrichment factor of the $N@C_{60}$ sample (~10^{-6}), we were able to obtain at

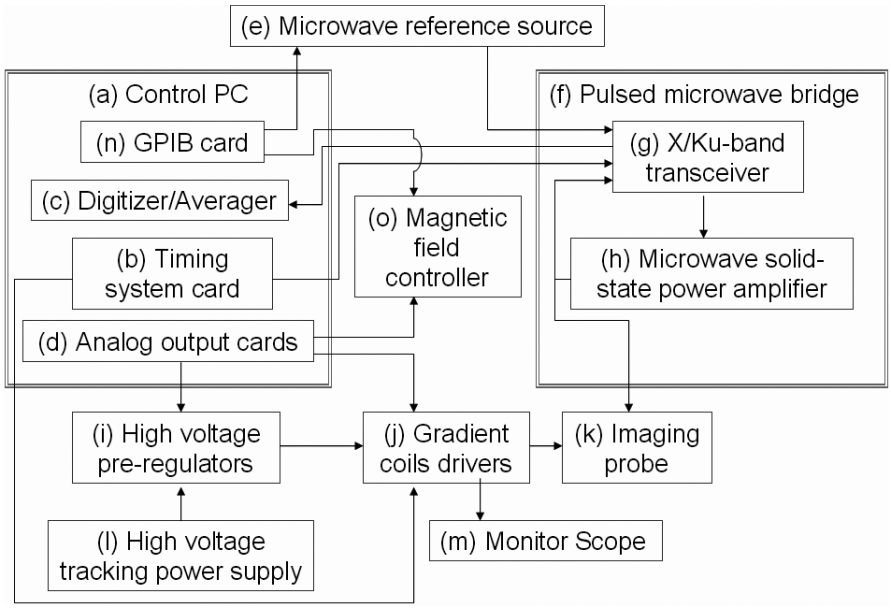

Fig. 2. A block diagram of the Pulsed ESR Imaging system.

room temperature images of $N@C_{60}$ with a resolution of only ~50 μm (with spin sensitivity of ~10^7 spins).

EXPERIMENTAL

CW ESR

Bruker CW ESR system (X-band EMX) was used to measure the CW ESR spectrum of solid $N@C_{60}$ and to evaluate the amount of spins in the $N@C_{60}$ sample with respect to a reference sample.

Pulsed ESR Imaging System

The measurements of T_1 and T_2, as well as the imaging experiments were all performed with our "home-built" Pulsed ESR imaging system. A block diagram of this system is presented in Fig. 2. The system is constructed from the following main components: (a) PC, which supervises the image acquisition process through LabView software (National Instruments); (b) Timing card (PulseBlasterESR-Pro from SpinCore), which has 21 TTL outputs, time resolution of 2.5 ns, and a minimum pulse length of 2.5 ns; (c) an 8-bit two-channel PCI-format digitizer card for raw data acquisition and averaging having a sampling rate of 500 MHz and averaging capability of up to 0.7 M waveforms/s (AP-235, Acqiris); (d) PCI analog output card having 8 outputs with 16-bit resolution (PCI-6733, National Instruments); (e) microwave reference source (HP8672A) with power output of 10 mW in the 2–18 GHz range; (f) a "home-built" pulsed microwave bridge containing (g) a 6–18 GHz low-power transceiver and (h) a solid-state power amplifier with 1 W output, 35 dB gain (home made); (i) high-voltage pre-regulator power supply for the (j) gradient coil drivers, which control the pulsed gradient coils in the imaging probe; (k) micro-imaging probe.

The imaging probe and its gradient coils are shown in Figs. 3 and 4. A rutile (TiO_2) microwave dielectric ring resonator with a diameter of 2.4 mm and height of 0.5 mm is fed by a coaxial line and placed with the sample in the center of the gradient coil structure. The gradients include a set of x, y, and z gradient coils. The structure of the x gradient coil is a simple Maxwell pair, the coils of the pair are connected in parallel and have total inductance of 1.1 μH, resistance of 0.5 Ohm, and produce magnetic gradient of 1.37 T/m•A. The y gradient coil is based on Goley geometry, has total inductance of 2.09 μH, resistance of 0.55 Ohm, and it produces a magnetic gradient of 1.25 T/m•A. Both the x and y gradient coils are driven by the pulse current drivers. The z-gradient coil is also based on Golay geometry and has efficiency 1.31 T/m•A. It has total inductance of 8.9 μH and resistance of 1.8 Ohm, making it more suitable for static gradient than for pulsed operation. The maximum magnetic field gradient achieved by this system (for the x and y coils) with short (0.5–1 μs) current pulses of 40 A (out of a 620 V source) is ~55 T/m. The shield (shown in Fig. 4, made of ~1-μm-thick golden foil) acts as a barrier that prevents the microwave from escaping out of the resonator but still enables the low-frequency field generated by the gradient coils to penetrate inside. This enables one to maintain a high

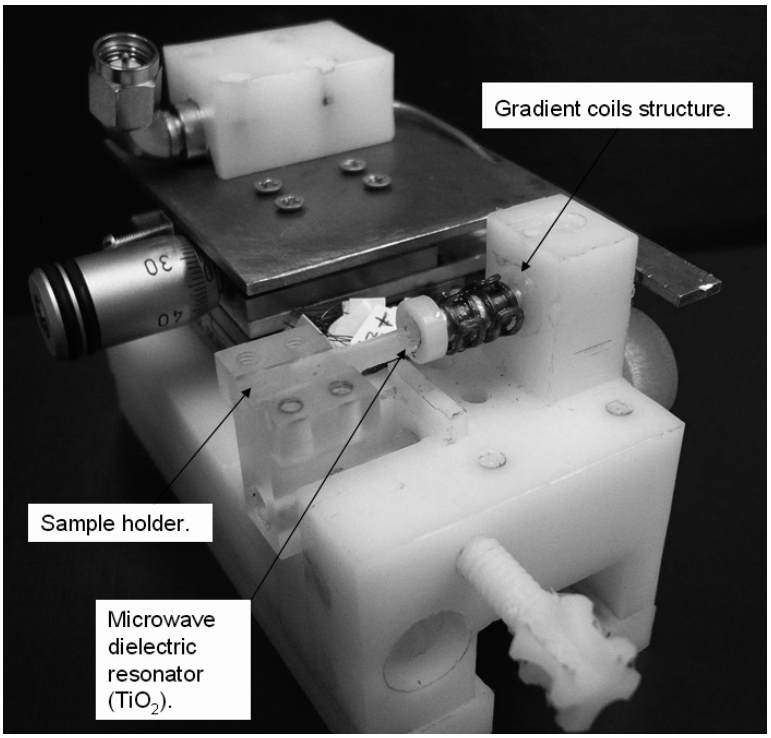

Fig. 3. The pulsed ESR imaging probe.

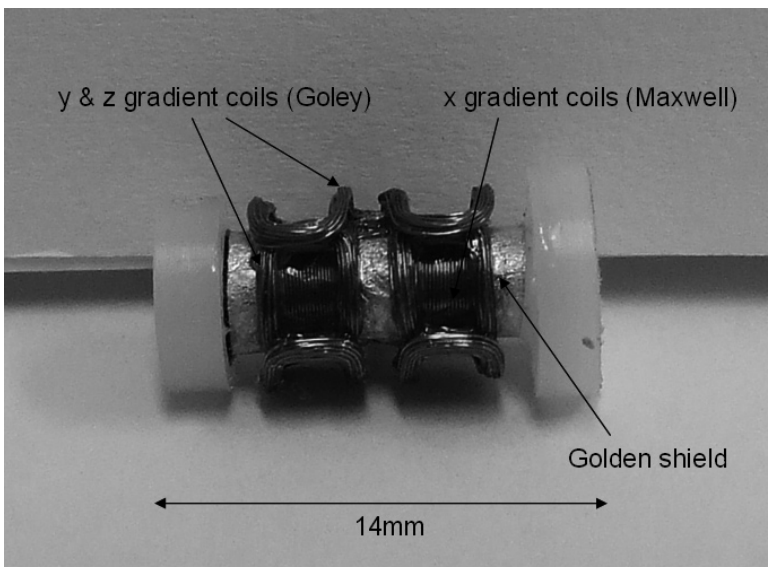

Fig. 4. Gradient coil structure.

quality factor for the microwave resonator, while still avoiding eddy currents due to the fast pulsed gradients. The system can be used either as a simple pulsed ESR spectrometer (when the gradients are not in use), or as an imaging system. In the latter case the imaging sequence shown in Fig. 5 was employed.[13]

Sample Preparation

Endohedral fullerene, $N@C_{60}$ (supplied by Prof. J.R. Cross from Yale) was dissolved in carbon disulfide (CS_2). The solution was evaporated to increase its concentration and was placed in a special glass sample holder, developed and prepared by our group via photolithography (Fig. 7B).[15] The unique design of the sample holder provides well-defined patterns for the imaging experiments and contributes to the enhancement in the sensitivity of the pulsed ESR imaging system. The sample contained approximately $\sim 10^{11}$ spins (evaluated by the CW ESR signal vs. reference signal of Trityl 1 μM solution).

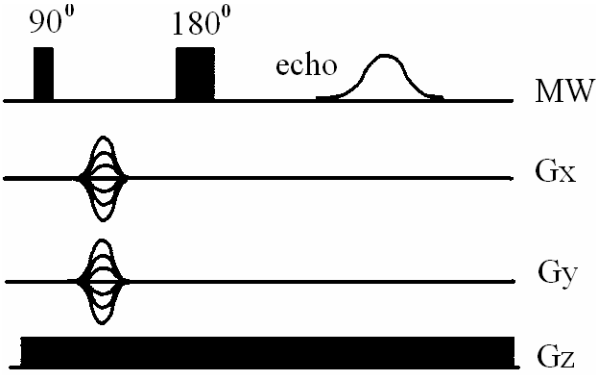

Fig. 5. Typical ESR pulse sequence used for imaging. The x and y pulsed gradients have a typical duration of ~0.7 μs, and peak magnitude of ~1.5 T/m. The constant z gradient has a magnitude of ~0.5 T/m.

RESULTS AND DISCUSSION

The N@C_{60} sample underwent a set of ESR measurements to verify its composition and to characterize its properties. As a first test we measured the CW spectrum of the sample with a commercial X-band system (Fig. 6A). The spectrum exhibits the familiar three sharp peaks induced by the nitrogen hyperfine splitting of 5.67 G.[16] The line width of the peaks was found to be relatively broad (~0.2 G) compared to previous measurements (0.05 G).[16] This is probably due to relatively large modulation employed (0.1 G), which was necessary in order to obtain a measurable signal. Saturation was not observed in the above measurement. The broad central peak is most likely due to C_{60} molecular fragments and

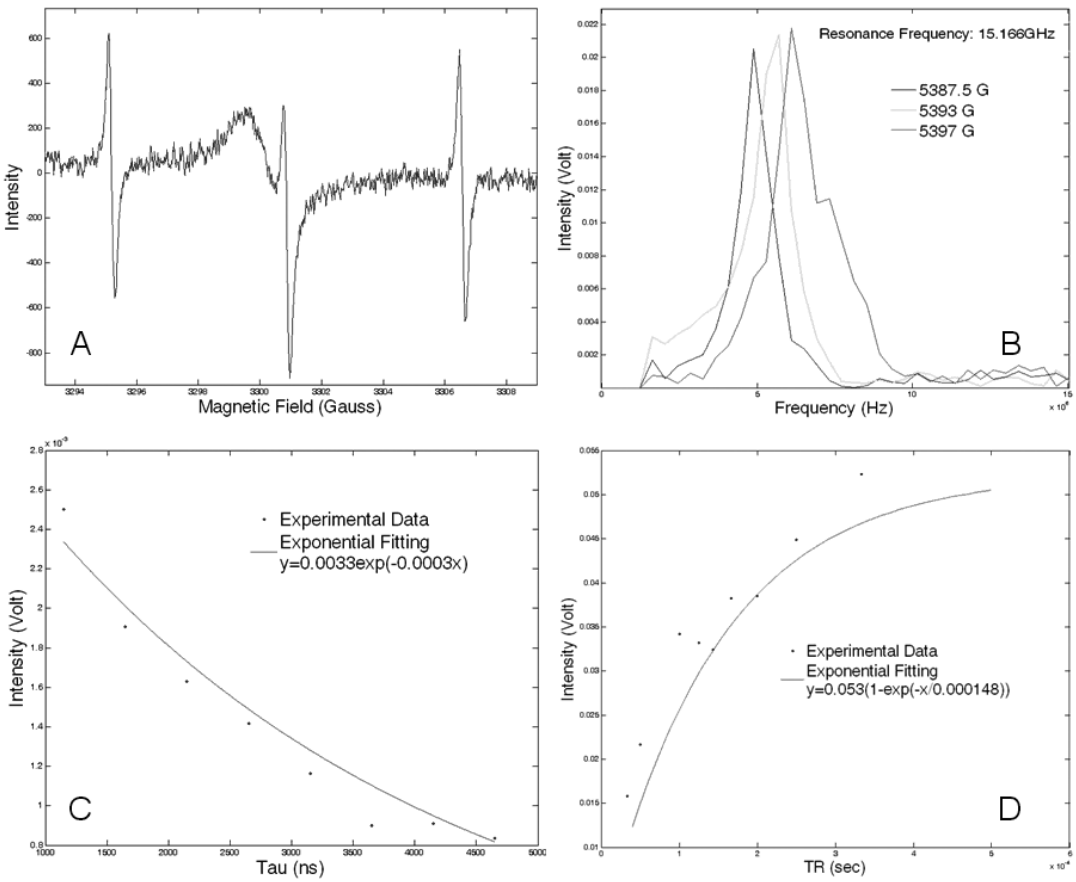

Fig. 6. (A) CW spectrum of a solid N@C_{60} sample. The typical line width of the sharp peaks is ~0.2 G. This spectrum was obtained at a frequency of ~9.2 GHz, modulation of 0.1 G, and attenuation 25 db (~1 mW of power). (B) Pulsed field step echo spectrum of the N@C_{60} sample (spectrum show in the frequency domain). (C) T_2 measurement: primary echo sequence was used to measure the spin–spin relaxation time, the peak amplitude of the echo was measured as a function of τ (the interval between the first and the second pulse). The relaxation time was calculated from the following relation: $V(\tau) \propto \exp(2\pi/T_2)$ The spin–spin relaxation time was found to be 6 ± 0.56 μs. (D) T_1 measurement: for the spin–lattice relaxation time measurement Free-Induction-Decay (FID) sequence was used with a single 90° pulse. The peak amplitude in the frequency domain was measured as a function of the repetition time (T_R). The relaxation time was evaluated from the following relation: $V(T_R) \propto (1 - \exp(-T_R/T_1))$, where $V(T_R)$ is the peak amplitude for specific repetition time. The spin–lattice relaxation time was found to be 148 ± 17 μs.

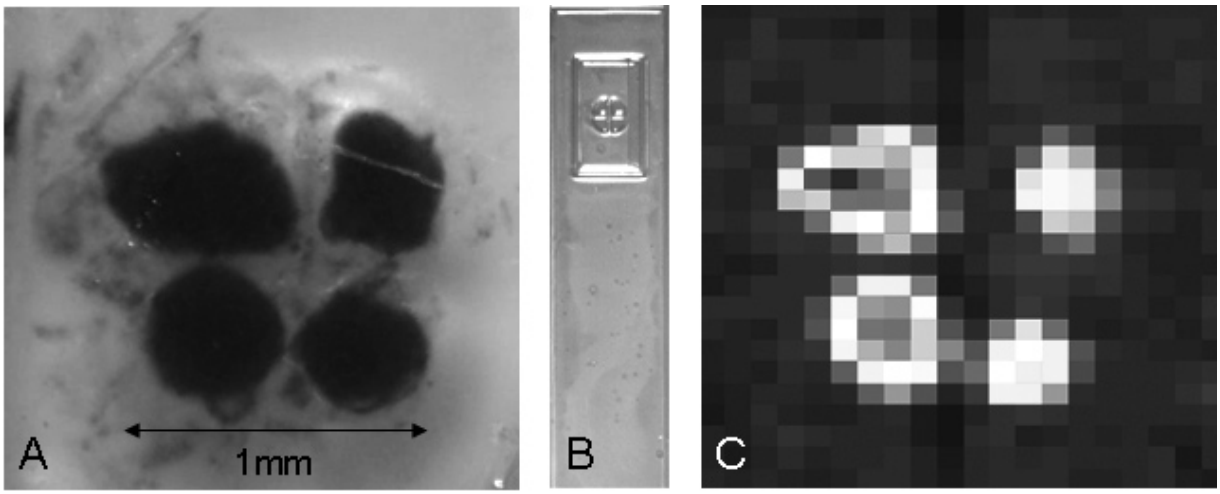

Fig. 7. (A) N@C_{60} solid sample used for imaging. (B) Glass sample holder produced by photolithography. (**C**) Pulsed ESR Image of a solid N@C_{60} sample dispersed on a surface (zoom in on the sample, showing part of the original 64 × 64 pixel image).

other impurities in the sample. Based on the ESR signal we estimated the number of spins in the sample to be ~10^{11} with an enrichment factor of ~10^{-6}.

Following the CW experiments, a set of pulsed ESR measurements was conducted to verify the capability of our home-built system to obtain a measurable signal and to quantify the sample relaxation times (T_1, T_2). Figure 6B shows the measured field step echo signal (three field values) that is in good agreement with the CW spectrum in terms of peak separation (~5.5 G). The broad peak that appears in the CW spectrum, which has much shorter T_2, could not be observed in the pulse measurements. The high sensitivity of our resonator, along with the inherent advantages of the pulse vs. CW system, were useful for the quantification of the sample T_1 and T_2 parameters (Figs. 6C,D). The values obtained in our measurements for T_1 and T_2 (148 μs and 6 μs, respectively) are not in full agreement with those appearing in the literature (120 μs and 20 μs, respectively).[3] The main discrepancy appears in the value of T_2, which is shorter than previous measurements, possibly due to dipole–dipole interactions by the paramagnetic impurities in the sample and the use of different Larmor frequency in our experiments (16.8 vs. 94 GHz in the literature).[17]

Following this basic sample characterization work, more advanced micro-imaging experiments were carried out. A standard imaging pulse sequence (Fig. 5) was employed for the acquisition of the N@C_{60} image (Fig. 7C). The imaging sequence is based on two MW pulses of 90° and 180° (with durations of 100 ns and 140 ns, respectively), resulting in a primary echo signal. The spatial encoding is achieved by employing a constant gradient for the sample z-axis and two pulse gradients for the y- and x-axes. This sequence was repeated every ~T_1. The experiments were performed at room temperature and at a frequency of 16.8 GHz. The total ESR image acquisition time was ~1.5 h to increase signal-to-noise ratio (SNR). The number of pixels for the entire 2D image was 64 × 64, and the calculated single pixel SNR is between 7–10. Image resolution was found to be ~50 μm by comparing the length and width of the ESR image (measured in pixels) to the actual size of the sample inside the resonator volume of interest (measured in mm).

CONCLUSIONS AND FUTURE DIRECTIONS

The present experimental effort resulted in a rather low resolution of ~50 μm, which is relatively poor compared to some of our previous experiments (leading up to 3-micron resolution).[13] This is due to the low enrichment factor (~10^{-6}) of the sample used here, which limited the SNR of the measurement. Theoretically the enrichment factor can approach 100% (we already have access to samples with 1% enrichment), which implies a maximum of ~10^6 increase in SNR. Since the gradient strength can be greatly increased by electronic improvements, one can safely assume that currently the resolution is limited only by the SNR per voxel. It is known that the voxel SNR is linearly proportional to the voxel volume (i.e., the number of spins). Thus, increased SNR

would open the way to the imaging of smaller voxels. For 2D images there is a square root dependence between the SNR and the pixel linear size, $\Delta x = \sqrt{SNR}$, implying that for the fully enriched sample the 2D resolution can be improved by a factor of ~1000. In addition to improving sample composition, further improvements are planned for the imaging system itself. The gradient coil shield in the probe is being replaced from a simple foil (having non-uniform texture and thickness) to a well-defined layer produced by Physical Vapor Deposition (PVD). This provides a thin uniform cover of gold (~1 μm) on top of a smooth glass tube. It significantly increases the quality factor of the resonator relative to the use of a simple gold foil, while still minimizing possible eddy currents caused by the pulsed magnetic field gradients. Furthermore, a cryogenic system will be constructed to enable work at a low temperature of ~4 K. At this temperature, apart from the Boltzmann factor improvement, the dielectric crystal of the resonator (rutile, TiO_2) has a much higher quality factor (more than 10,000). Finally, the microwave system will be extended to work at the frequency ranges of 35 GHz and 60 GHz, which would result in reduced resonator size and a further increase in sensitivity and image resolution. These collective measures would enable the detection of very few $N@C_{60}$ spins, approaching single-spin sensitivity, with spatial resolution of tens of nm,[14] which can be attractive for QC applications.

Acknowledgments. This work was partially supported by grant numbers 169/05 and 1143/05 from the Israel Science Foundation, and by a grant from the Russell Berrie Nanotechnology Institute at the Technion. We gratefully acknowledge Prof. J.R. Cross (Yale University) for supplying us with the $N@C_{60}$ sample. The help of Yael Talmon with preparation of photolithographic glass sample holders is also greatly appreciated.

REFERENCES AND NOTES

(1) Morton, J.J.L.; Tyryshkin, A.M.; Ardavan, A.; Porfyrakis, K.; Lyon, S.A.; Briggs, G.A.D. *Phys. Rev. B* **2007**, *76*, No. 085418.
(2) Weidinger, A.; Waiblinger, M.; Pietzak, B.; Murphy, T.A. *Appl. Phys. A* **1998**, *66*, 287–292.
(3) Harneit, W.; Meyer, C.; Weidinger, A.; Suter, D.; Twamley, *J. Phys. Status Solidi B-Basic Res.* **2002**, *233*, 453–461.
(4) Harneit, W. *Phys. Rev. A* **2002**, *65*, 032322.
(5) Suter, D.; Lim, K. *Phys. Rev. A* **2002**, *65*, No. 052309.
(6) Shu-Shen, L.; Gui-Lu, L.; Feng-Shan, B.; Song-Lin, F.; Hou-Zhi, Z. *Proc. Natl. Acad. Sci. USA* **2001**, *98*, 11847–11848.
(7) Preskill, J. *Quantum Computing: Pro and Con;* ITP Conference on Quantum Coherence and Decoherence, California Institute of Technology, Pasadena, USA, 1997.
(8) Steane, A. *Rept. Prog. Phys.* **1998**, *61*, 117–173.
(9) Vandersypen, L.M.K.; Steffen, M.; Breyta, G.; Yannoni, C.S.; Sherwood, M.H.; Chuang, I.L. *Nature* **2001**, *414*, 883–887.
(10) Schmidt-Kaler, F.; Haffner, H.; Riebe, M., Gulde, S.; Lancaster, G.P.T.; Deuschle, T.; Becher, C.; Roos, C.F.; Eschner, J.; Blatt, R. *Nature* **2003**, *422*, 408–411.
(11) Kane, B.E. *Nature* **1998**, *393*, 133–137.
(12) Suetsuna, T.; Dragoe, N.; Harneit, W.; Weidinger, A.; Shimotani, H.; Ito, S.; Takagi, H.; Kitazawa, K. *Chem.—Eur. J.* **2002**, *8*, 5079–5083.
(13) Blank, A.; Dunnam, C.R.; Borbat, P.P.; Freed, J.H. *Appl. Phys. Lett.* **2004**, *85*, 5430–5432.
(14) Blank, A.; Freed, J.H. *Isr. J. Chem.* **2006**, *46*, 423–438.
(15) Halevy, R.; Talmon, Y.; Blank, A. *Appl. Magnet. Reson.* **2007**, *31*, 589–596.
(16) Franco, L.; Ceola, S.; Corvaja, C.; Bolzonella, S.; Harneit, W.; Maggini, M. *Chem. Phys. Lett.* **2006**, *422*, 100–105.
(17) Knorr, S.; Grupp, A.; Mehring, M.; Waiblinger, M.; Weidinger, A. *AIP Conf. Proc.* **2001**, *544*, 191–194.